Nonlinear Suppression of Range-Ambiguous Clutter for Outdoor Radar Measurement Facilities

THESIS

Michael Craig Baumgartner, Captain, USAF

AFIT/GE/ENG/06-06

DEPARTMENT OF THE AIR FORCE
AIR UNIVERSITY

AIR FORCE INSTITUTE OF TECHNOLOGY

Wright-Patterson Air Force Base, Ohio

AFIT/GE/ENG/06-06

Nonlinear Suppression of Range-Ambiguous Clutter for Outdoor Radar Measurement Facilities

THESIS

Presented to the Faculty

Department of Electrical and Computer Engineering

Graduate School of Engineering and Management

Air Force Institute of Technology

Air University

Air Education and Training Command

In Partial Fulfillment of the Requirements for the

Degree of Master of Science in Electrical Engineering

Michael Craig Baumgartner, B.S.E.E.

Captain, USAF

March 2006

AFIT/GE/ENG/06-06

Nonlinear Suppression of Range-Ambiguous Clutter for Outdoor Radar Measurement Facilities

Michael Craig Baumgartner, B.S.E.E.
Captain, USAF

Approved:

/signed/	13 Mar 2006
Maj Todd B. Hale, PhD (Chairman)	Date
/signed/	13 Mar 2006
Dr. Michael A. Temple (Member)	Date
/signed/	13 Mar 2006
Dr. Stephen C. Cain (Member)	Date

AFIT/GE/ENG/06-06

Abstract

In the outdoor measurement facility, a certain amount of real estate is owned by the organization, and therefore can be groomed to keep clutter contributions to a minimum. However, as the transmit signal travels further downrange, returns from long-range clutter sources are inevitable and can have significant impact on measurement accuracy. This research effort investigates the effectiveness of employing nonlinear suppression (NLS) to abate long-range ambiguous clutter in these facilities. In the simple two-pulse case, NLS requires a pulse repetition frequency which divides the radar's maximum range into two unambiguous ranges, and a transmit signal comprised of alternating nearly orthogonal pulses. Received signals are therefore a composite of the pulse interacting with the unambiguous portion of the range, and its complement interacting with the ambiguous. Matched filtering to the ambiguous pulse focuses (compresses) the clutter energy, and those portions of the return with magnitudes exceeding a threshold are set to zero. The process is completed by passing the remaining signal through the inverse matched filter, then matched filtering to the unambiguous pulse. The aim of NLS process is to remove as much ambiguous energy as possible while maintaining the maximum unambiguous energy. Thresholding techniques used by Anderson [1] are utilized and expanded upon. Initial testing provides an extended proof-of-concept for coincident point scatterers representing target and clutter sources. The process is finally applied to simulated measured data from the National Radar Test Facitily(NRTF), where five cases representing various target versus clutter signal power ratios are tested. Ratios are selected to cover the range of clutter signals having 0.25 to 4 times the power of the target signal. Results show promise for employing NLS in this arena, as one of the techniques studied retained on average 95% of the target signal power while discarding 78% of the ambiguous signal power.

Acknowledgements

I dedicate this humble body of work to my wife and children. I am forever indebted to you all for putting up with my missed meals, late nights and even missed nights. To the love of my life: your unending support and encouragement helped me to press on when I regularly felt like giving up. All too often you were forced to be both parents, and you shouldered the extra burden lovingly and without hesitation. You are *amazing.* Thanks to my lovely daughter for your incredible sense of humor and understanding when I couldn't always stick around to play as much as we both would have liked. You're a great kid, and I often think I learn more from you and your brother than I ever could from my research. Finally to my son: you've been a true joy since the day you arrived. Thanks for reminding me every day of what's really important in this life. I acknowledge that the sacrifices you all made are far greater than I may ever understand and appreciate. I love you all.

On an professional level, I'd like to express my sincerest gratitude to Maj Todd Hale, PhD, for his mentorship, guidance and often unwarranted confidence in me. Your leadership and support during unmentioned personal issues is deeply appreciated and speaks volumes to your character. You are a good man, and I feel I've become a better man for simply knowing you. Thank you.

My sincerest thanks as well to Dr. Mike Temple. My success in this endeavor is due largely to your countless hours of pro bono tutelage. Your words of wisdom (Temple-isms) will likely ring in my ears for the rest of my days. It depends... I'll have to think about it... It is what it is.

Michael Craig Baumgartner

Table of Contents

List of Figures

List of Tables

List of Symbols

Symbol		Page
$\odot$	Point by point multiply	10
$\tilde{y}_U[n]$	Performance model mismatch filtered unambiguous pulse	10
$\tilde{y}_A[n]$	Performance model match filtered ambiguous pulse	10
$y_N[n]$	Operational NLS output	10
$y_A[n]$	Performance model NLS ambiguous output	11
$y_U[n]$	Performance model NLS unambiguous output	11
P_u	Unambiguous signal power	11
P_a	Ambiguous signal power	11
$\frac{P_u}{P_a}$	Power unambiguous to power ambiguous ratio	11
$h'[n]$	Impulse response of terrain reflectivity	28
h_{ave}	Mean terrain impulse response	28
σ	Standard Deviation	28
ϕ	Phase	29
$h[n]$	Terrain impulse response	30
$r_U[n]$	Received unambiguous signal	35
D	Target scaling constant	35
$r_A[n]$	Received ambiguous signal	35
$r[n]$	Received composite signal	35
$\bar{\alpha}$	Floating treshold	36
$\bar{\alpha}_{Fixed}$	Fixed ideal threshold	36

List of Abbreviations

Nonlinear Suppression of Range-Ambiguous Clutter for Outdoor Radar Measurement Facilities

I. Introduction

Outdoor radar cross section (RCS) measurement facilities have a unique capability of being able to measure large (often non-scaled) targets. The tradeoff for this flexibility lies in having a somewhat unstable clutter scene. While environmental factors within the immediate vicinity of the range can be controlled, the long-range clutter scene can be in a constant state of flux and provides a ready source of measurement errors. The terrain in a desert environment, for example, changes at a steady pace as sand blows and drifts. Unfortunately, unlike indoor ranges, the outdoor facility is unable to implement a simple background subtraction scheme to minimize these ambiguous clutter areas. The National Radar Test Facility (NRTF) is one such facility and is the sponsor of this work. The overarching research goal is to minimize the received energy from long-range ambiguous clutter areas in hopes of enhancing measurement fidelity.

Non linear suppression (NLS) is a technique introduced by Palmero et al in 1962 and was revisited extensively by Anderson in 2001 [1]. In previous works, NLS has been used primarily to suppress clutter in target detection scenarios. While proven effective in this arena, its usefulness has yet to be understood when applied to static RCS measurements. Thus, this body of work represents an extension to the progress made by Anderson and attempts to demonstrate NLS effectiveness in the outdoor RCS measurement facility.

1.1 Conventions, Nomenclature and Limitations

All waveforms considered in this work are simulated in the `MATLAB®` environment, and therefore a continuous-time signal $s(t)$ is referred to by its sampled discrete-

time representation $s[n]$. All sampling during simulations is done at a minimum of twice the Nyquist rate, which is defined in [3] as two times the signal bandwidth. Also, please note that throughout this document, "target," "target pulse"and "unambiguous pulse" are used interchangeably, as are "clutter," "clutter pulse" and "ambiguous pulse."

Finally, NRTF has provided the topic considered but methods proposed herein are not currently implementable at their facility. Specifically, waveforms employed in later chapters prove technique viability, but are not supported by hardware in place at NRTF at the time of this work.

1.2 Organization

Chapter II acquaints the reader with the concept of range ambiguities and recounts in the author's own words, Anderson's development of the NLS process. Topics covered also include thresholding techniques, waveform selection and performance metrics.

Chapter III expands Anderson's model to focus on the NRTF measurement environment. An extended proof-of-concept is presented which explores the effectiveness of NLS using single point scatterer targets appearing at the same ambiguous range. Performance is analyzed for multiple relative magnitudes between target and clutter impulses. A sample image of measured data from NRTF is presented and a process developed to use the image to create an unlimited number of "pseudo-measured" data sets.

Chapter IV introduces possible techniques for adjusting thresholds, then evaluates NLS performance using 1000 realizations for each of 5 input power ratios. Finally, conclusions are drawn in Chapter V, as well as recommendations for future endeavors.

II. Nonlinear Suppression Basics

This chapter fills a basic toolbox which is needed to understand and apply nonlinear suppression (NLS). A brief discussion of range ambiguities is followed by an introduction to NLS fundamentals. Thresholding techniques, waveform selection and performance analysis from [1] are presented to complete the picture.

2.1 Range Ambiguities

To understand the theory of nonlinear suppression, an understanding of the basic concept of range ambiguity is required. In a vast majority of radar applications, a *series* of pulses is transmitted at a given pulse repetition interval (PRI), which has a corresponding pulse repetition frequency (PRF). The PRI (T_p) is related to the PRF (f_p) by

$$T_p = \frac{1}{f_p}. \tag{2.1}$$

Figure 2.1 shows 6-pulses of a simple rectangular signal with a PRI of 500 ns and PRF of 2 MHz. Figure 2.2 shows this signal interacting with two ideal point scatterers that

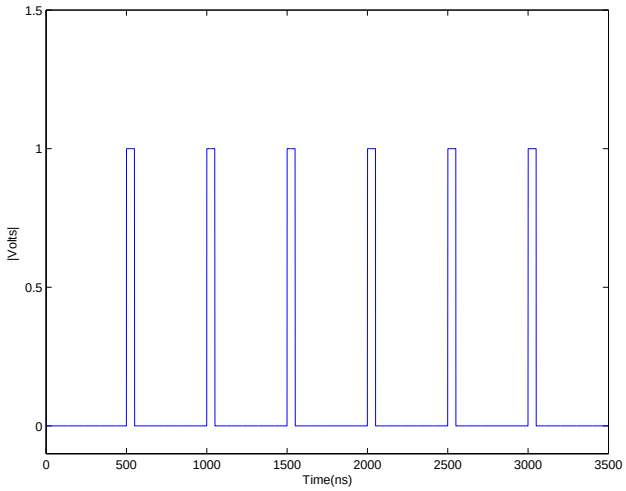

Figure 2.1: Transmitted Radar Signal with $PRF = 2$MHz.

are located exactly $\frac{T_p}{2}$ apart. This figure provides a simple illustration of the concept

of range ambiguity. The first returned pulse (p1) has only target 1 (t1) information, denoted by p1t1 in the lower plot of Fig.2.2. When p2 is received it not only contains t1 information (p2t1) but also the interaction of p1 with t2 (p1t2) as well. In the case of the second pulse, this p1t2 contribution is range-ambiguous, i.e., it *appears* at the same range as t1 but actually exitis an additional $\frac{cT_p}{2}$ meters downrange ($c \approx 3e^8$, the speed of light).

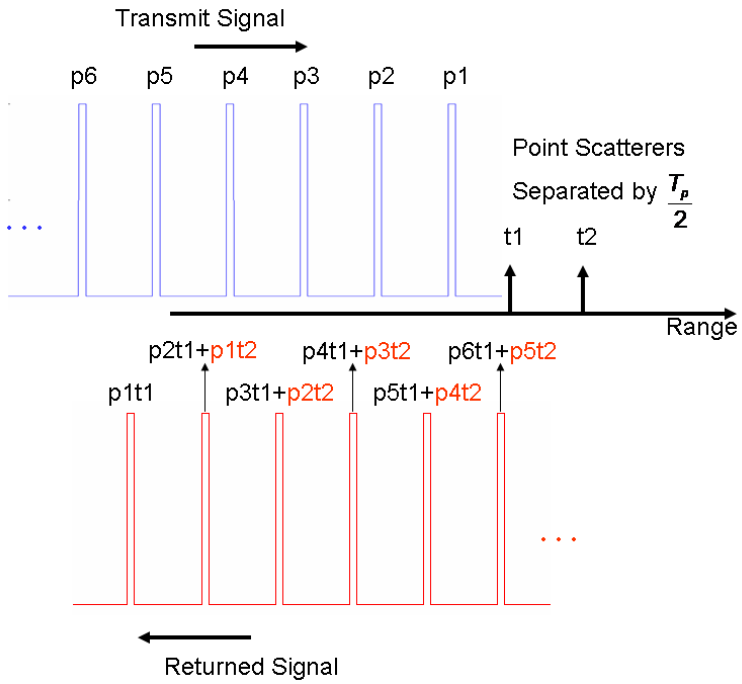

Figure 2.2: Transmitted rectangular pulse interrogating two targets separated by a distance equal to $\frac{T_p}{2}$. Returned signal pulses (red) are labelled to illustrate foldover of range-ambiguous energy. For example, p2t1 + p1t2 is pulse 2 interacting with target 1 plus the ambiguous return of pulse 1 interacting with target 2.

The illustration in Fig. 2.2 nicely frames the concept of maximum unambiguous range, R_{un}, which is defined as the range beyond which targets appear as second time around echoes [3]. Unambiguous range is given by

$$R_{un} = \frac{c}{2f_p}. \tag{2.2}$$

Stated perhaps more simply, as long as the extent in range being considered is less than R_{un}, no second time around (range-ambiguous) echoes will exist. Applying Eqn. (2.2) to the waveform in Fig. 2.1 results in a maximum unambiguous range of 75 meters.

It would seem at this point that the problem is solved: simply reduce the PRF to a rate which ensures no second time around echoes exist. While effective in eliminating ambiguities, measurement range time is extremely expensive. Thus, reducing the PRF makes this proposition cost-prohibitive and further drives the need to explore options like NLS.

2.2 Nonlinear Suppression (NLS) Fundamentals

The NLS framework is readily understood using a simple two-pulse illustration. Let $s[n]$ represent the transmit signal, which has a PRF such that the maximum range visible by the radar is $R_{\text{max}} = 2R_{\text{un}}$. Two unique waveforms are alternately applied when creating $s[n]$. For example, one pulse is coded using linear frequency modulation (LFM) with an up-chirp (LFMup), and the next by LFM with a down-chirp (LFMdn).

! Waveform selection is NOT ARBITRARY. Details on the process are found in Section 2.4.

An illustration of $s[n]$ interacting with one target and one clutter source is illustrated by Fig. 2.3. The received signal in this scenario has both target and clutter information superimposed within each pulse. Due to the total scene being divided into $2R_{\text{un}}$, if the received pulse $r_m[n]$ contains LFMup-coded target data, it also contains LFMdn-coded clutter data. The alternating pattern of $s[n]$ then dictates that $r_{m+1}[n]$ contains LFMdn-coded target and LFMup-coded clutter data. This pattern continues to alternate for the duration of the received signal.

Nonlinear suppression requires a matched filter in the receiver for each uniquely coded pulse in the transmit signal. In this scenario, one is matched to LFMup, denoted by h_{LFMup} and the second to LFMdn (h_{LFMdn}). The first step in processing received

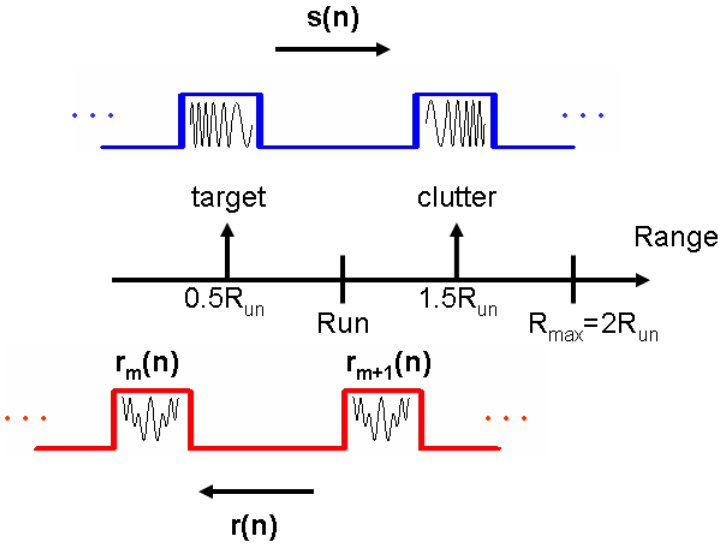

Figure 2.3: Alternating LFM transmit signal and composite return signal. For target and clutter point scatterers spaced as shown, each composite received pulse contains a combination of alternately-coded target and clutter data.

data using NLS is to match filter to the pulse containing the ambiguous information, as seen in Fig. 2.4. If implemented in an actual radar, the switch shown would likely be toggled by a delay-line, adjusted relative to the range of interest. This process simply tracks which waveform is interacting with the ambiguous portion of the range.

After the first matched filter $\mathbf{h}$, the next block in Fig 2.4 represents the nonlinearity designed to suppress range-ambiguous data. During this nonlinear operation, any portion of the filtered received signal $\tilde{y}_m[n]$ exceeding a threshold α is set to zero, ideally removing all ambiguous signal energy. This technique is used extensively in [1] and is referred to as the hole-punching function, $\Gamma_\alpha(\tilde{y}_m[n])$, given by

$$\Gamma_\alpha(\tilde{y}_m[n]) = \begin{cases} 0 & \text{if } |\tilde{y}_{\mathrm{m}}[n]| > \alpha \\ \tilde{y}_{\mathrm{m}}[n] & \text{otherwise} \end{cases} \text{, for m} = 0 \text{ , } 1. \tag{2.3}$$

This nonlinear function is graphically illustrated by Fig. 2.5.

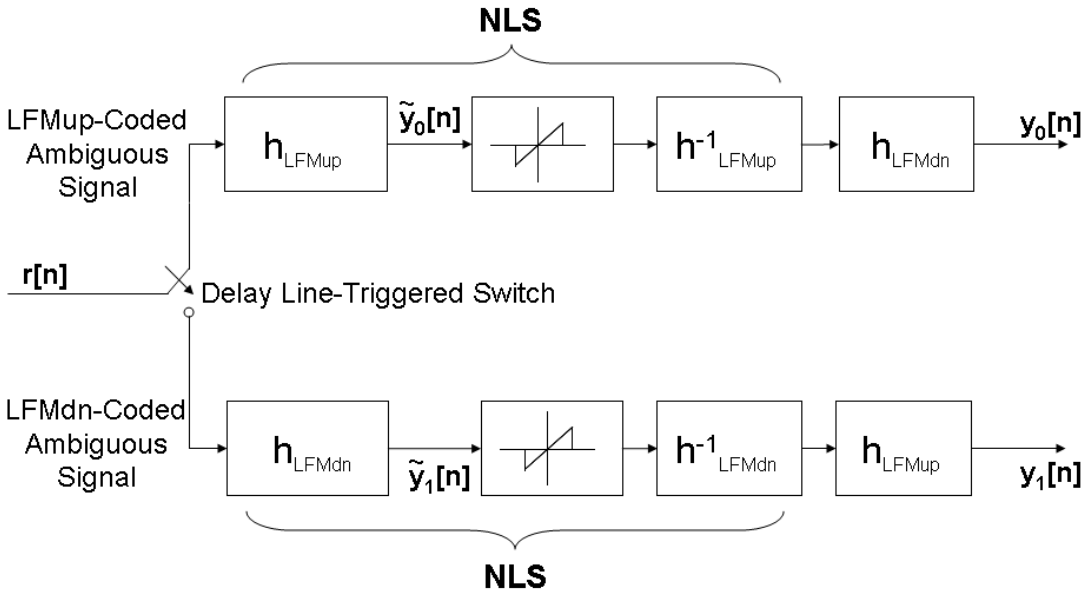

Figure 2.4: Two channel nonlinear suppression scheme. As labelled, a delay line tracks which waveform interacts with the ambiguous terrain and toggles the switch appropriately. The first matched filter ($\mathbf{h}$) compresses the ambiguous pulse and the nonlinearity ideally removes all ambiguous signal energy. The inverse filter ($\mathbf{h^{-1}}$) restores the remaining unambiguous pulse before a final matched filter focuses the desired target signal.

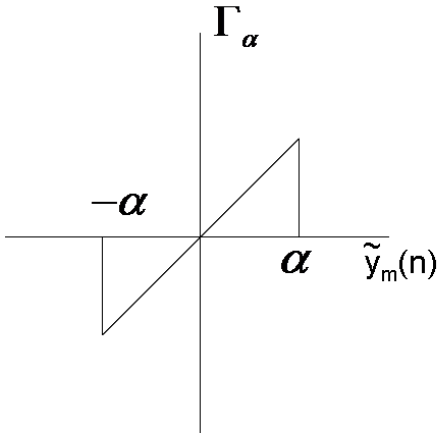

Figure 2.5: Hole-punch nonlinearity. When $|\tilde{y}_m[n]| > \alpha$, $\tilde{y}_m[n]$ is set to zero.

Considering the upper channel of Fig. 2.4, the step following the nonlinearity reverses the effects of the first matched filter using an inverse filter ($\mathbf{h^{-1}}$), the conjugate reflection filter for $\mathbf{h}$ [1]. This filter de-focuses the remaining clutter signal energy and restores the desired target portion of the signal to its original received form, completing the NLS process. The final processing in Fig. 2.4, which is not part of the NLS operation, is a filter matched to the target waveform. This represents the sole matched filter a receiver chain would normally utilize had NLS not been added to the "front end" of the system. If implemented properly, at this point the majority of the clutter signal energy has been removed, while maintaining maximum target signal integrity. At this point it is apparent that the success of this entire process relies heavily on the thresholding technique.

2.3 NLS Thresholding Techniques

With a basic understanding of NLS in hand, special attention is given to the process of thresholding. Three techniques are presented by Anderson [1] for use in two-channel NLS: the constant threshold, locally constant threshold and local average threshold (LAT). While Anderson immediately discards the constant threshold, the latter pair are explored in great detail. No declaration is made as to which is most effective and performance of each proved nearly identical for multiple phase-coding schemes. As a result, the LAT is arbitrarily chosen for thresholding in this work. The local average is simply a scaled average magnitude of $\tilde{y}_m[n]$, the composite received signal match filtered to the ambiguous waveform, over $2b+1$ samples. The point-wise LAT $\alpha[n]$ is given by:

$$\alpha[n] = \frac{a}{2b+1} \sum_{k=n-b}^{n+b} |\tilde{y}_m[k]|, \text{ for } m = 0, 1. \tag{2.4}$$

Since $\tilde{y}_m[n]$ is matched to the clutter signal, regions containing strong clutter responses are sharply focused (energy concentrated in a relatively few samples). The

local average exploits these peaks by taking an average magnitude over several surrounding samples. This averaging sets the threshold below the strong clutter areas, precipitating their removal. Near the ends of $\tilde{y}_m[n]$, the average is calculated using fewer samples. The scale factor a and sampling factor b are adjusted to optimize LAT effectiveness.

> ! Please note that the sum $(2b+1)$ is referred to herein as the "sampling width" throughout the remainder of this document. This is not to be confused with Nyquist sampling or the actual radar's sampling rate.

2.4 Waveform Selection

Essential to NLS effectiveness is employing groups of signals with highly dispersed cross-correlation and sharply focused autocorrelation responses. As shown in Chapter III, sharply focussed autocorrelation allows clutter signal energy to be pinpointed and subsequently removed by the hole-punch nonlinearity with minimal disruption of the target pulse. The well dispersed cross-correlation further enhances this effectiveness by spreading desired target signal energy, again providing minimal disruption of the target pulse. Anderson goes to great lengths to characterize performance of numerous phase-coding techniques, which include Gold codes, M-Sequences and those generated by a simulated annealing algorithm. Touted as providing"near optimum" results, Anderson uses LFM-coded signals to characterize baseline performance [1]. Therefore, waveforms used in all testing scenarios that follow are limited to LFM.

2.5 Performance Analysis

The toolbox is nearly complete, as NLS fundamentals, thresholding and waveforms are in place. The final step is to pull everything together to characterize performance. Anderson developed a vital evaluation model for NLS, shown with minor modifications for clarity in Fig. 2.6. This model provides a solid foundation for several useful metrics. Model inputs are the received ambiguous (clutter) signal $r_A[n]$ on the

upper channel and unambiguous (target) signal $r_U[n]$ on the lower. Following Anderson's design, these signals contain purely ambiguous and unambiguous range data, respectively, and are created by coding distinct range intervals with unique pulses. Both signals are passed through a filter matched to the ambiguous (clutter) waveform, h_A, given by

$$h_A[n] = s_A^*[-n], \tag{2.5}$$

as defined in [2], and where $s_A[n]$ is the transmitted ambiguous waveform. The lower channel now contains a dispersed target-only response, which after taking its magnitude and applying the scale factor a' is termed the ideal threshold, α_I:

$$\alpha_I[n] = a'|\tilde{y}_U[n]|, \tag{2.6}$$

where $\tilde{y}_U[n] = s_U[n] * h_A[n]$, and $*$ represents convolution.

> ! It is important to note that the ideal threshold is for *performance evaluation only*, in contrast to the local average threshold, which is considered an *applied* technique.

Since all operations at this point are linear, the summation of $\tilde{y}_U[n]$ and $\tilde{y}_A[n]$ is equivalent to a received composite signal match filtered to the ambiguous waveform. This summation may now be used along with α_I to create what Anderson calls the hole-punch vector [1], defined as

$$\mathbf{V}_\alpha[\mathbf{n}] = \begin{cases} 0 & \text{if } |\tilde{y}_U[n] + \tilde{y}_A[n]| > \alpha_I[n] \\ 1 & \text{otherwise.} \end{cases} \tag{2.7}$$

Next, the series of zeros and ones contained in $\mathbf{V}_\alpha[\mathbf{n}]$ are multiplied point-by-point (the $\odot$ operator) with both $\tilde{y}_U[n]$ and $\tilde{y}_A[n]$. The zeros correspond to elements where the composite signal exceeded α_I. The sum of these hole-punched signals is passed through the conjugate reflection filter to produce the signal $y_N[n]$, which is

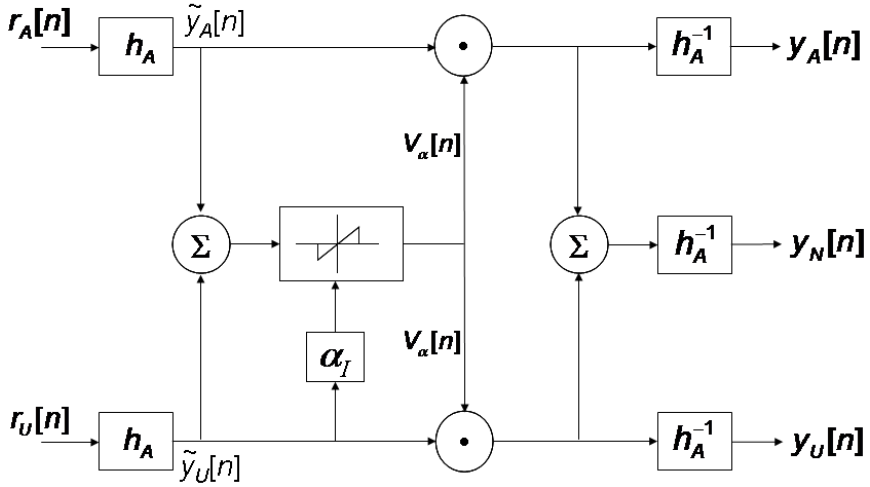

Figure 2.6: NLS Performance Evaluation Model

equivalent to the output of an operational NLS channel. Flanking $y_N[n]$ in Fig. 2.6 are the ambiguous output $y_A[n]$ and the unambiguous output $y_U[n]$.

The first of Anderson's performance metrics is a ratio of the unambiguous (P_u) to ambiguous (P_a) signal powers:

$$\frac{P_u}{P_a} = \frac{\sum_{n=0}^{N-1} |y_U[n]|^2}{\sum_{n=0}^{N-1} |y_A[n]|^2}. \tag{2.8}$$

At first glance it may appear as if something is missing in eqn. (2.8), as power is defined as signal energy over a time interval. Since both target and clutter power are calculated over the same interval, these time units cancel. This ratio of $\frac{P_u}{P_a}$ is often compared to the same ratio at the input of the radar, given by

$$\text{Input}\frac{P_u}{P_a} = \frac{\sum_{n=0}^{N-1} |r_U[n]|^2}{\sum_{n=0}^{N-1} |r_A[n]|^2}. \tag{2.9}$$

Both ratios are referred to in the appropriate context as the "power ratio." Comparing the input power ratio to the NLS output power ratio provides the first indication of NLS effectiveness.

The final two metrics are the Suppressed Power Ratio-Ambiguous (SPRA) given by

$$SPRA = \frac{P_a|_{T=\alpha}}{P_a|_{T=\infty}} = \frac{\sum_{n=0}^{N-1} |y_A[n]|_{T=\alpha}|^2}{\sum_{n=0}^{N-1} |y_A[n]|_{T=\infty}|^2}, \tag{2.10}$$

and the Suppressed Power Ratio-Unambiguous (SPRU), given by

$$SPRU = \frac{P_u|_{T=\alpha}}{P_u|_{T=\infty}} = \frac{\sum_{n=0}^{N-1} |y_U[n]|_{T=\alpha}|^2}{\sum_{n=0}^{N-1} |y_U[n]|_{T=\infty}|^2}. \tag{2.11}$$

Both the SPRA and SPRU are a ratio of power after NLS using the ideal threshold, to power using an infinite threshold. The latter case is equivalent to bypassing the hole-punching operation altogether, and ensures the filter "coloration" effects are included when making a head-to-head comparison of the results. SPRU values near 1 are desirable as this indicates the majority of power from the target pulse is retained. Similarly, an SPRA approaching 0 reveals the majority of the undesired clutter energy is removed. It may be helpful to think of these metrics as percentages. For the SPRU, a value of 0.96 indicates that 96% of the target signal power is retained, and an SPRA of 0.22 reveals 78% of clutter signal power is rejected.

Given performance metrics are in place, as are the basic tenets of nonlinear suppression, a sufficient foundation now exists to extend previous research and apply NLS to the outdoor measurement environment.

III. NLS in the RCS Range Environment

This chapter explores the effectiveness of nonlinear suppression (NLS) for co-incident point scatterers of various relative magnitudes. An additional performance metric is introduced, which provides a means to more accurately adjust thresholds. A process is developed to utilize a single snapshot of measured data to create as many data sets as needed for testing scenarios.

3.1 Expanding the Model

During the proof-of-concept phase presented in Anderson's Chapter II [1], he did not present instances where single point scatterer target and clutter sources are at the exact same unambiguous range. The extremely stable environment of the outdoor measurement facility nearly guarantees an appreciable range-ambiguous return from long-range clutter will *appear* at the same range as the target for a multitude of pulse repetition frequencies (PRFs). Therefore, an extension of Anderson's proof-of-concept for point scatterers is in order. This time, target and clutter appear co-incident when the clutter return is folded over.

Figure 3.1 (a) shows the focused (match-filtered or autocorrelation) response of a point scatterer which represents a radar cross section (RCS) measurement target. Figure 3.1 (b) is the dispersed (mismatch-filtered or cross-correlation) response of a second point scatterer of the same magnitude, which represents the range-ambiguous clutter return.

A total of five Input$\frac{P_u}{P_a}$ power ratios are considered: -6 dB, -3 dB, 0 dB, 3 dB, and 6 dB. These values provide scenarios ranging a from target return having 4 times the power of the clutter return, down to a target having 0.25 times the power. Both ideal and local average thresholding are considered. A third method, termed multiple local average threshold (MLAT) is tested as well. MLAT may be literally interpreted as simply establishing the local average threshold (LAT) and performing the hole-punching operation, then repeating the thresholding/hole-punching process

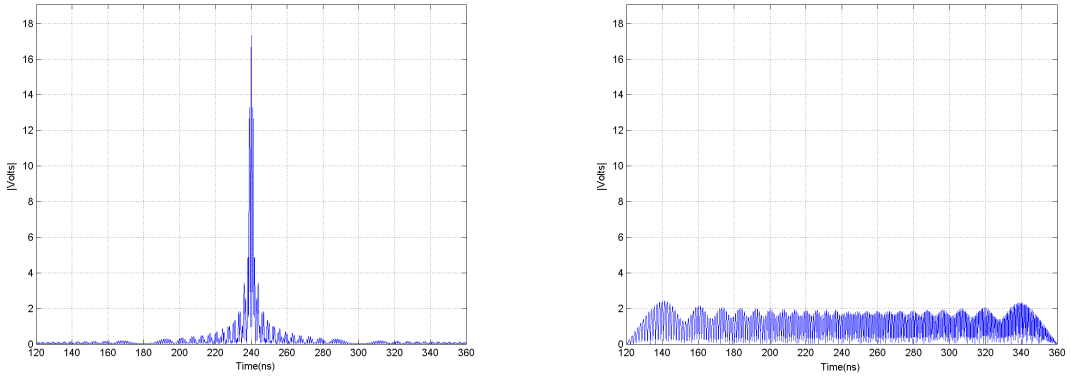

(a) (b)

Figure 3.1: (a) Focused (match-filtered) unambiguous pulse.
(b) Dispersed (mismatch-filtered) ambiguous pulse.

several times. The aim is to incrementally remove the ambiguous signal energy in an attempt to retain as much of the unambiguous energy as possible.

Figure 3.2 shows the composite signal match-filtered to the ambiguous waveform along with the ideal threshold. The zoom window illustrates how succinctly this method follows the contours of the composite signal. Recall that every portion of the composite signal above the threshold will be set to zero during the hole-punching operation of NLS.

While designed to evaluate performance using the ideal threshold, Anderson's evaluation model of Fig 2.6 is modified slightly to accommodate the applied thresholding techniques as well. This is possible since the composite received signal is artificially created by "folding over" ambiguous with unambiguous pulses, which are needed individually as inputs to the model. As shown in Fig. 3.3 for the single local average threshold (SLAT), the composite signal is now used to find the threshold α, and the remaining process is untouched. The model (not shown) is nearly identical for the MLAT, with a loop added to accommodate iteration of the thresholding and hole-punching operations.

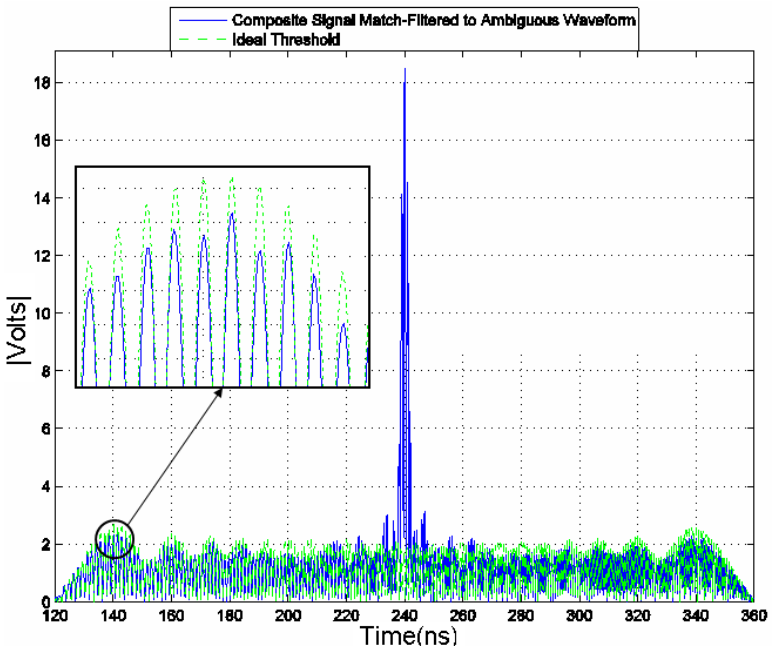

Figure 3.2: Composite signal (Input $\frac{P_u}{P_a}$ = 0.00dB) match-filtered to ambiguous pulse with overlaid ideal threshold.

Figures 3.4 through 3.8 show results of a single-pass LAT followed by successive iterations of the MLAT, all for Input $\frac{P_u}{P_a} = 0.00$ dB. Threshold scale factors and sampling width were optimized in all cases for a favorable (minimized) suppressed power ratio-ambiguous (SPRA). Note in Fig. 3.4 that the threshold falls below the composite signal sidelobes for much of the duration. NLS based on this threshold not only reduces ambiguous signal energy, but could remove a considerable amount of unambiguous signal energy as well. In contrast, the MLAT thresholds in Figs. 3.5 through 3.7 leave a majority of sidelobes completely intact and therefore result in increased unambiguous signal integrity. Table 3.1 gives final performance for both methods, where the $\Delta\frac{P_u}{P_a}$ term reflects the improvement or degradation in the power ratio after NLS. In this instance, the MLAT technique yields a marked improvement, as $\frac{P_u}{P_a}$ at the output exceeds the single pass increase by 1.31 dB. Recall SPRA values approaching zero indicate nearly all ambiguous signal energy is removed and suppressed power ratio-unambiguous (SPRU) values near one represent a largely intact unambiguous pulse.

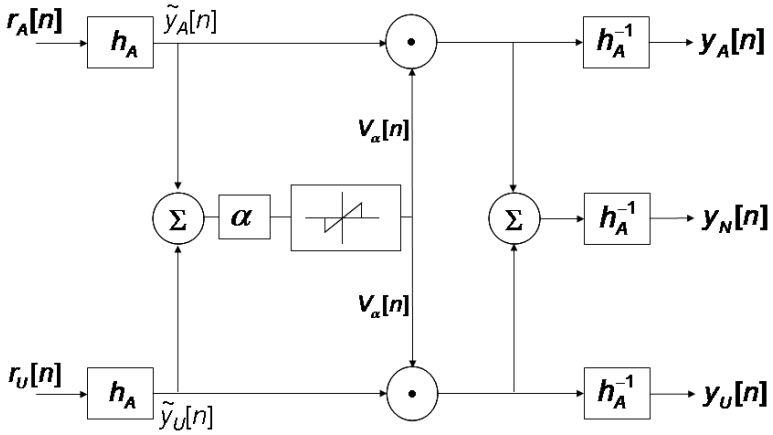

Figure 3.3: NLS performance evaluation model modified for the single local average threshold.

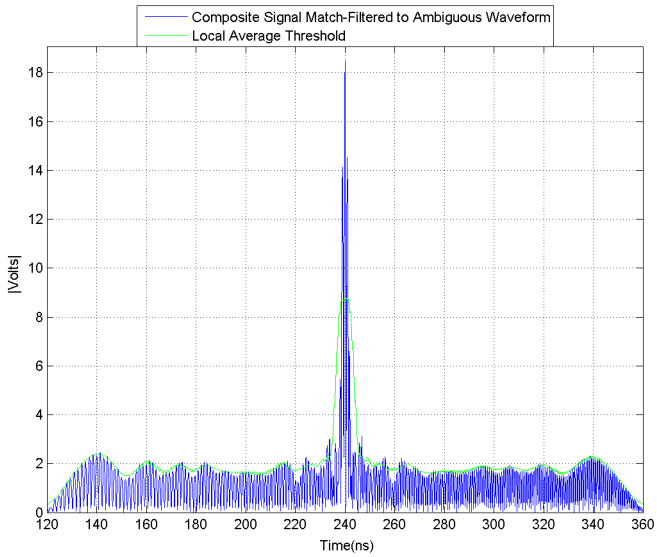

Figure 3.4: Composite signal (Input $\frac{P_u}{P_a} = 0.00$dB) match-filtered to ambiguous pulse with overlaid single local average threshold.

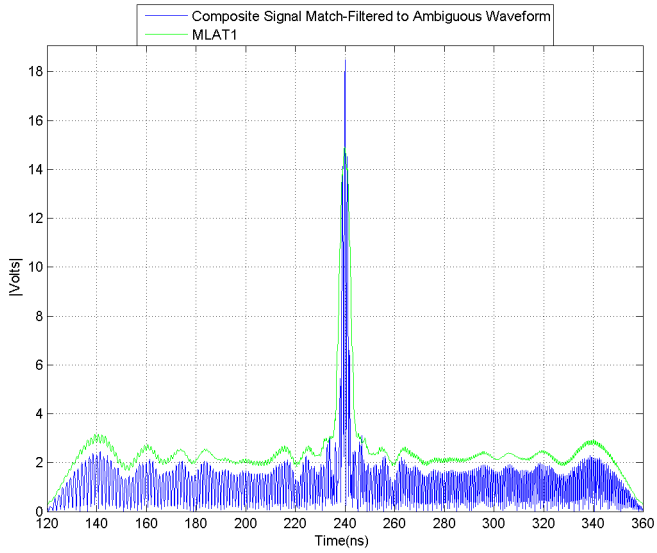

Figure 3.5: Composite signal (Input $\frac{P_u}{P_a} = 0.00$dB) match-filtered to ambiguous pulse with overlaid first pass MLAT.

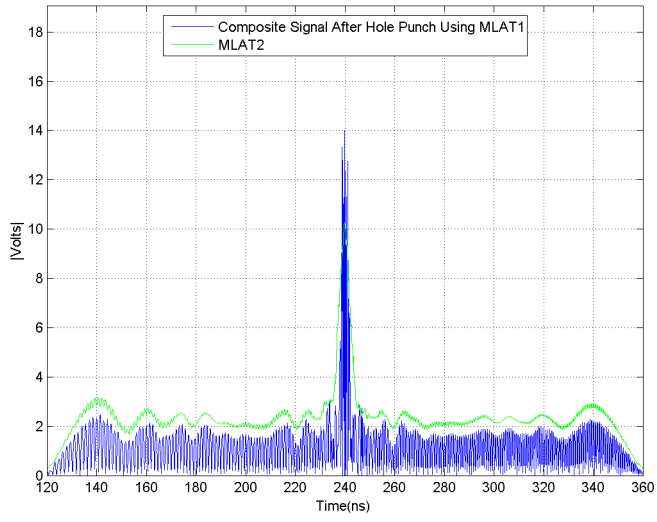

Figure 3.6: Composite signal (Input $\frac{P_u}{P_a} = 0.00$dB) after first hole-punching operation with overlaid second pass MLAT.

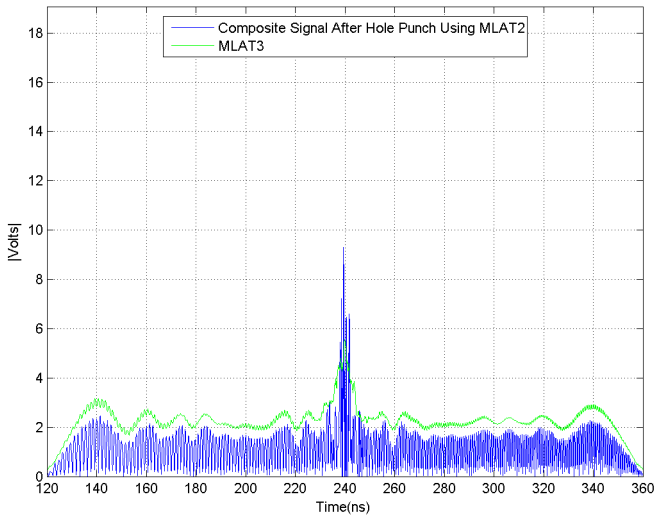

Figure 3.7: Composite signal (Input $\frac{P_u}{P_a} = 0.00$dB) after second hole-punching operation with overlaid third pass MLAT.

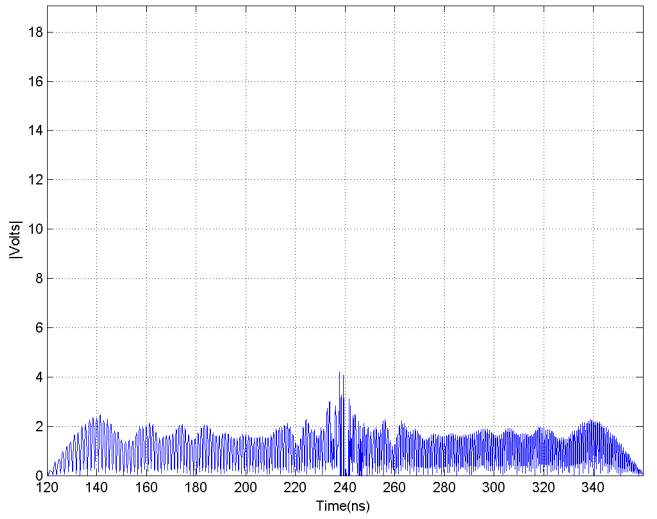

Figure 3.8: Composite signal (Input $\frac{P_u}{P_a} = 0.00$dB) match-filtered to ambiguous pulse after complete MLAT.

While not quantitatively assessed, Figs. 3.9 and 3.10 reveal by inspection that the single and multiple LAT techniques produce very similar results in the Input $\frac{P_u}{P_a} =$ 0.00 dB case. For a more robust comparison, Fig. 3.11 is a cumulative magnitude difference ($|\Delta|$) between the individual results of each thresholding technique and the match-filtered unambiguous target pulse. This focused target pulse is used for comparison since it represents the"pure return" (ie no range-ambiguities) attainable if the PRF were cut in half. When plotted, a lower cumulative difference indicates a waveform that better matches the contour of the target-only pulse. The difference tracing for the composite signal match-filtered to the unambiguous pulse is shown for completeness and to accent the power of NLS.

NLS is now performed for all Input $\frac{P_u}{P_a}$ ratios proposed earlier. In each case, threshold scale factors and sampling widths are adjusted to maximize the SPRU. Table 3.2 shows the results of all methods. Both thresholding techniques produce and improvement in output $\frac{P_u}{P_a}$, and at times show performance nearing the ideal threshold. Overall, it appears that the MLAT technique may offer some improvement over the single threshold in cases where the target return is stronger than clutter, but performs poorly in the high clutter power scenarios.

Until now the decision to maximize SPRU (to retain maximum target power) or minimize SPRA (to reject maximum clutter power) has been completely arbitrary. A balance can be struck between keeping a minimum clutter signal energy while maintaining maximum contribution from the target pulse. If the measurements are taken with the simple intent of gathering RCS magnitude data (versus an imaging

Table 3.1: NLS single point scatter target performance for single LAT vs. MLAT, (Input $\frac{P_u}{P_a} = 0.00$dB).

	Single Local Ave Thresh			Multi Local Ave Thresh		
Input $\frac{P_u}{P_a}$(dB)	$\Delta\frac{P_u}{P_a}$(dB)	SPRU	SPRA	$\Delta\frac{P_u}{P_a}$(dB)	SPRU	SPRA
0.00	+9.66	0.778	0.084	+10.97	0.983	0.079

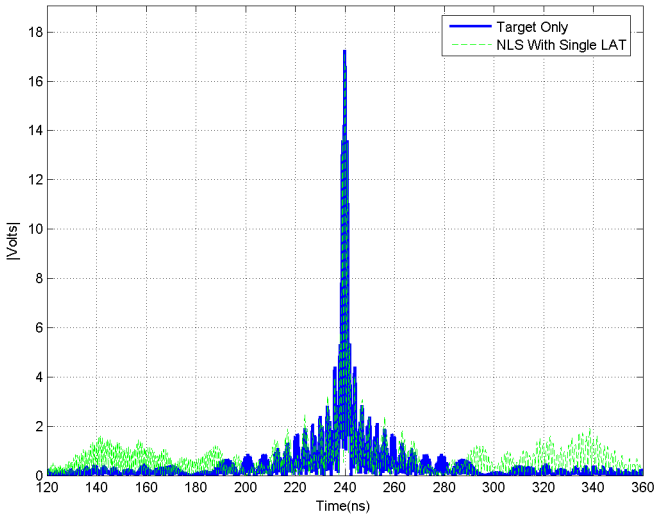

Figure 3.9: Comparison of unambiguous signal and composite signal (Input $\frac{P_u}{P_a}$ = 0.00dB) after single LAT NLS, both match-filtered to unambiguous waveform.

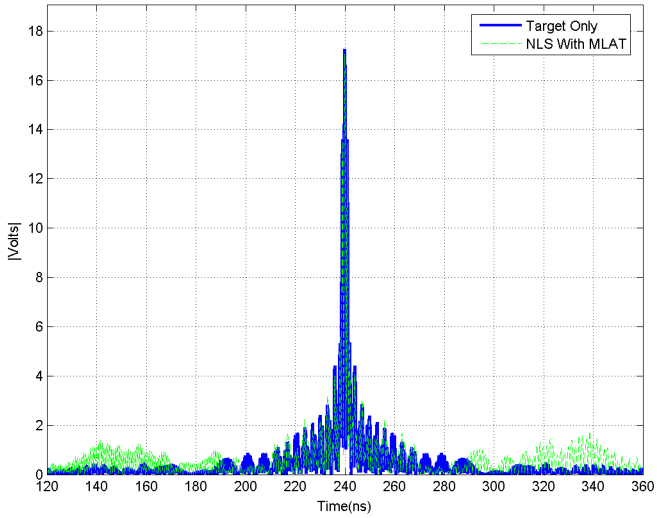

Figure 3.10: Comparison of unambiguous signal and composite signal (Input $\frac{P_u}{P_a}$ = 0.00dB) after MLAT NLS, both match-filtered to unambiguous waveform.

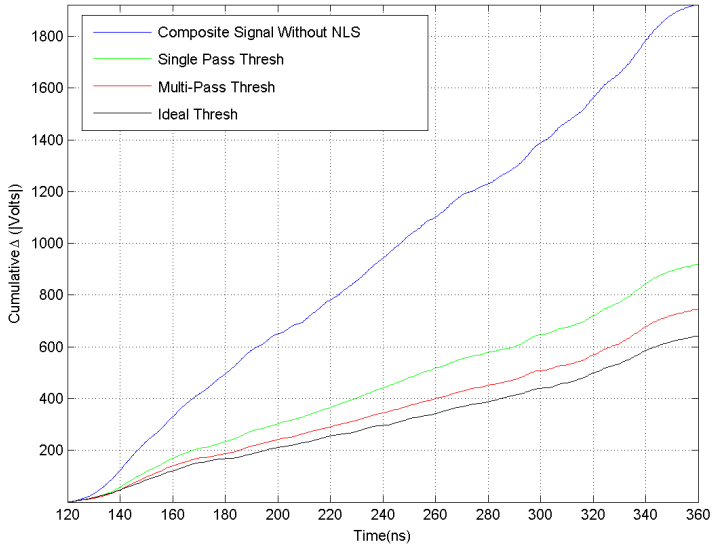

Figure 3.11: Cumulative point-by-point $|\Delta|$ for all thresholding techniques. The $|\Delta|$ is measured from a match-filtered target pulse, and reveals how well NLS-processed waveforms follow the contour of "pure" data. All thresholds are adjusted for maximum SPRU.

Table 3.2: Ideal Threshold vs. Single Local Average and Multiple Local Average Threshold Performance On Single Point Scatterer Target and Clutter. Thresholds in all cases adjusted to maximize SPRU.

	Ideal Threshold				Single Local Ave Thresh		
Input $\frac{P_u}{P_a}$(dB)	$\Delta\frac{P_u}{P_a}$(dB)	SPRU	SPRA		$\Delta\frac{P_u}{P_a}$(dB)	SPRU	SPRA
-6.02	+8.42	0.996	0.143	$\Rightarrow$	+7.99	0.996	0.158
-2.97	+8.30	0.996	0.147	$\Rightarrow$	+5.53	0.996	0.279
0.00	+8.31	0.996	0.147	$\Rightarrow$	+5.54	0.996	0.279
3.02	+8.30	0.996	0.147	$\Rightarrow$	+5.53	0.996	0.279
6.02	+9.4	0.996	0.114	$\Rightarrow$	+5.53	0.996	0.279

	Ideal Threshold				Multi Local Ave Thresh		
Input $\frac{P_u}{P_a}$(dB)	$\Delta\frac{P_u}{P_a}$(dB)	SPRU	SPRA		$\Delta\frac{P_u}{P_a}$(dB)	SPRU	SPRA
-6.02	+8.42	0.996	0.143	$\Rightarrow$	+2.43	0.996	0.570
-2.97	+8.30	0.996	0.147	$\Rightarrow$	+4.32	0.996	0.368
0.00	+8.31	0.996	0.147	$\Rightarrow$	+7.11	0.997	0.194
3.02	+8.30	0.996	0.147	$\Rightarrow$	+7.11	0.997	0.194
6.02	+9.4	0.996	0.114	$\Rightarrow$	+5.53	0.996	0.279

application), a fourth useful metric is the total power ratio (TPR), given by

$$\text{TPR} = \frac{P_u|_{T=\alpha} + P_a|_{T=\alpha}}{P_u|_{T=\infty}} = \frac{\sum_{n=0}^{N-1} |y_U[n]|_{T=\alpha}|^2 + \sum_{n=0}^{N-1} |y_A[n]|_{T=\alpha}|^2}{\sum_{n=0}^{N-1} |y_U[n]|_{T=\infty}|^2}. \tag{3.1}$$

The TPR simply shows how the total power of the NLS channel output compares to the power in the unambiguous pulse, which can be considered truth data the NLS process is attempting to approach. TPR values of 1 are ideal, values less than 1 reveal excessive signal energy removed during NLS and values greater than 1 too little. Analyzing the TPR in concert with the SPRU provides the most complete picture. A TPR *and* SPRU near 1 would indicate the best possible NLS performance.

The simulations represented in Table 3.2 are re-run, adjusting threshold scaling and sampling width to bring the TPR as near to unity as possible. Results are shown in Table 3.3. The value of considering the TPR when adjusting threshold constants is evident in the considerable improvement across the board in $\Delta\frac{P_u}{P_a}$. When compared to optimizing based on SPRU alone, the ratio increased an average of 5.73 dB. Note that in both the ideal and MLAT simulations, the ratio improves as clutter power increases. While a curious observation, care must be taken to consider the whole picture, as SPRU values have decreased at the same time. The lesson is that while there is an appearance of improved performance with increased clutter strength, the reality may be that only the ratio $\frac{P_u}{P_a}$ has improved. An improved $\frac{P_u}{P_a}$ is by itself a favorable outcome in target detection, but could prove costly in terms of accuracy in RCS measurements. Further supporting this theory is the fact that the SPRU is considerably degraded at the same time.

In all instances, MLAT NLS now outperforms the single pass suppression, with an increase in $\Delta\frac{P_u}{P_a}$ values ranging from 1.58 dB to 5.49 dB better than the single pass. Note also that‘ MLAT SPRU remains much nearer the desired value of 1, and the SRPA nearer to 0 in all cases. Figure 3.12 shows nice improvement in waveform accuracy for all methods when adjusting thresholds based on the TPR and SPRU. As

compared to thresholding based solely on the SPRU, the cumulative $|\Delta|$ final values for all techniques are roughly cut in half.

After examining nonlinear suppression as applied to coincident point scatterers, the process appears to have great promise in the RCS measurement setting. With thresholding techniques further refined, the next step is to explore the measured data provided by the sponsor and prepare it for further simulations.

Table 3.3: Ideal Threshold vs. Single Local Average and Multiple Local Average Threshold Performance On Single Point Scatterer Target and Clutter. TPR = 1.00 in all Instances.

	Ideal Threshold				Single Local Ave Thresh		
Input $\frac{P_u}{P_a}$(dB)	$\Delta\frac{P_u}{P_a}$(dB)	SPRU	SPRA		$\Delta\frac{P_u}{P_a}$(dB)	SPRU	SPRA
-6.02	+17.79	0.939	0.016	$\Rightarrow$	+9.52	0.693	0.077
-2.97	+16.33	0.957	0.022	$\Rightarrow$	+10.05	0.837	0.083
0.00	+14.45	0.970	0.035	$\Rightarrow$	+10.29	0.917	0.086
3.02	+13.63	0.979	0.042	$\Rightarrow$	+9.03	0.944	0.118
6.02	+12.63	0.987	0.054	$\Rightarrow$	+9.00	0.971	0.122

	Ideal Threshold				Multi Local Ave Thresh		
Input $\frac{P_u}{P_a}$(dB)	$\Delta\frac{P_u}{P_a}$(dB)	SPRU	SPRA		$\Delta\frac{P_u}{P_a}$(dB)	SPRU	SPRA
-6.02	+17.79	0.939	0.016	$\Rightarrow$	+15.01	0.893	0.028
-2.97	+16.33	0.957	0.022	$\Rightarrow$	+13.45	0.921	0.042
0.00	+14.45	0.970	0.035	$\Rightarrow$	+12.35	0.952	0.055
3.02	+13.63	0.979	0.042	$\Rightarrow$	+11.12	0.964	0.074
6.02	+12.63	0.987	0.054	$\Rightarrow$	+10.58	0.982	0.086

3.2 Exploring the Range Walk

Figure 3.13 shows an actual range walk collected at 10GHz. Data is collected by transmitting k pulses and hardware gating the received signal k times at 1 nanosecond increments. As a result, the plot shown represents $120,000$ (that is, $k = 120,000$) data points, displayed as range vs. RCS magnitude in decibels. Using a simple range equation $R = \frac{cT_p}{2}$ from [3], an apparent target is found at roughly $15,100$ ns or $2,263$ meters. Incidentally, no target was present when these measurements were taken - the

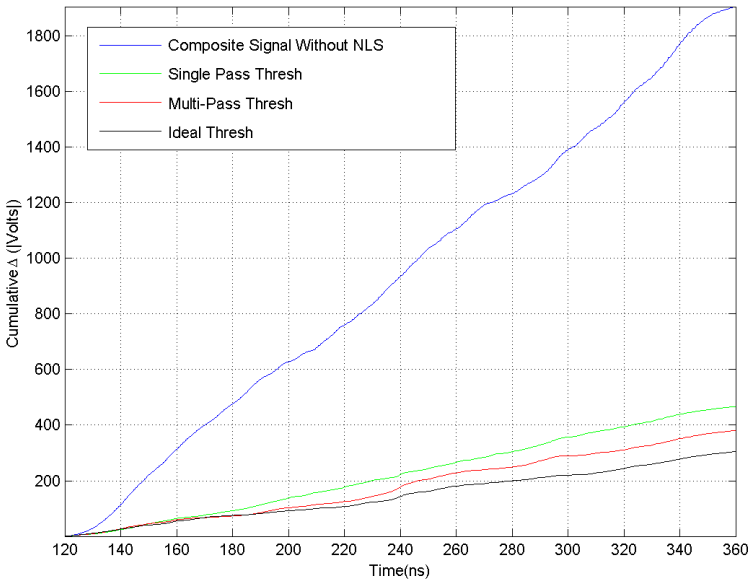

Figure 3.12: Cumulative point-by-point $|\Delta|$ for all thresholding techniques. The $|\Delta|$ is measured from a match-filtered target pulse, and reveals how well NLS-processed waveforms follow the contour of "pure" data. All thresholds adjusted for optimum TPR.

return seen comes from the Radar VHF/UHF Measurement System (RVUMS), a mobile system that was the range the day the data was collected. Had a target been present, it would have appeared near the $19,000$ ns mark. Further downrange, the clutter begins at approximately $45,000$ ns ($6,745$ meters) and ends at $100,500$ ns or $15,739$ meters. As labeled, this region will be referred to as the clutter hump. An illustration of the ground-bounce measurement scene at the National Radar Test Facility (NRTF) is depicted in Fig. 3.14. The interaction with the rise in elevation corresponds to the start of the clutter hump in Fig. 3.13. Photographs of one of the radar measurement facilities at NRTF are shown in Figs. 3.15 and 3.16.

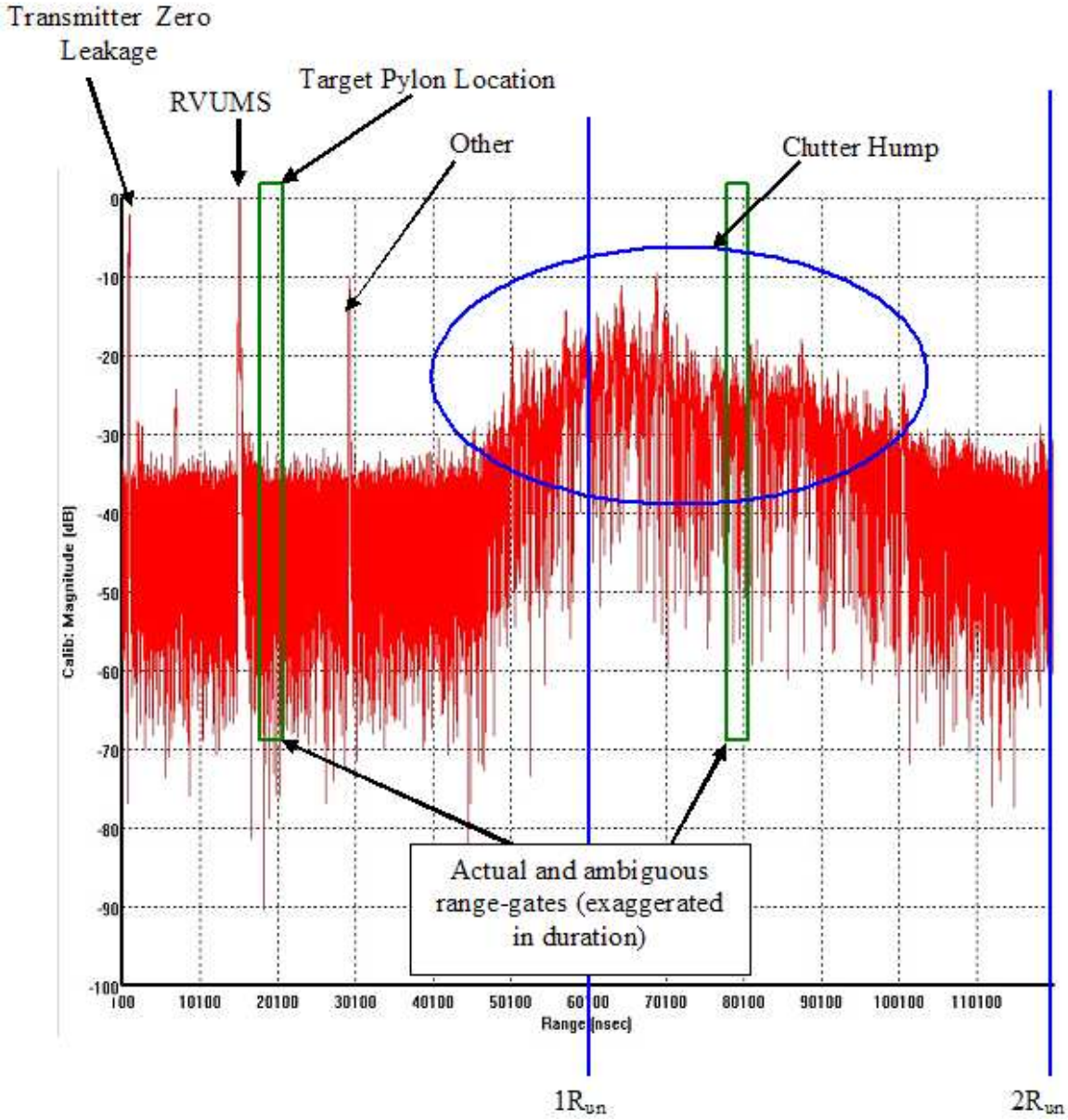

Figure 3.13: Range walk image collected with 10 GHz carrier, 85 ns pulse width.

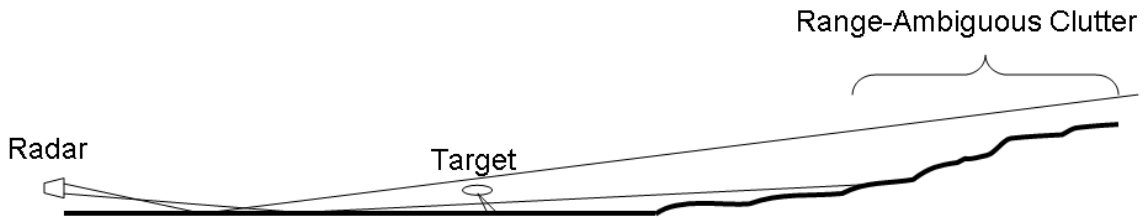

Figure 3.14: A not-to-scale conception of an outdoor radar measurement facility at NRTF. After interrogating the target, transmit signal eventually interacts with the rise in elevation.

For all simulations, the range is broken up into two ambiguous range swaths, shown on Fig. 3.13 as occurring every $60,000$ ns starting at $60,100$ ns. Going back to Eqn. (2.2), the appropriate PRF for this arrangement is found by first calculating the range at the end of the first swath.

$$\frac{c(60,100\text{ns})}{2} = 8,985\text{m} \tag{3.2}$$

Substitute this value for R_{un} in Eqn. (2.2) to solve for a PRF of approximately 16.6 KHz. Range gates are illustrated by green boxes in Fig. 3.13, which help to further define the problem at hand. Typical range gates are set at target range plus two times the target's maximum radius, plus some additional engineer-defined cushion. Targets with extensive cavities, for example, may be given a wider range gate to allow for all cavity returns to propagate back to the radar. A target with a maximum radius of 15 meters yields a nominal range gate of target range +30 meters, which corresponds in time to target range (in time) +100 ns. Within the majority of the first swath the noise floor remains relatively constant at around -35 dB. At around $45,000$ ns the ground first comes into view which is manifested by the start of the clutter hump shown in Fig. 3.13. Returns from ground clutter in this second swath are enclosed in the second green box, and result in a RCS considerably higher than the noise floor, peaking at approximately -20 dB.

Figure 3.15: This photo is taken looking downrange at NRTF, and gives a good perspective of the rise in elevation which contributes to the clutter problem.

Figure 3.16: Aerial photo of NRTF RCS measurement facility.

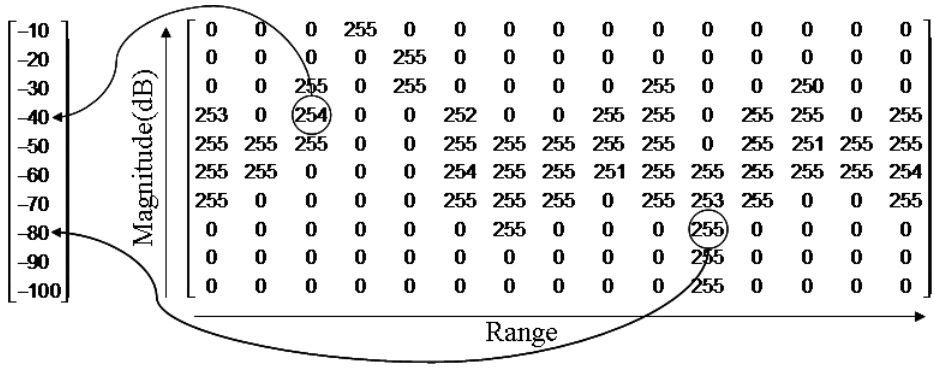

Figure 3.17: Mapping Technique for Data Image Matrix

3.3 Data Generation

Unfortunately, complex data from the sponsor radar was unavailable at the time of this work. In an effort to create multiple, realistic received radar signals, Fig. 3.13 is assumed to represent the impulse response of the terrain's reflectivity, $h'[n]$. While no phase data can be captured from the image, relative magnitudes of representative point scatterers are readily extracted. To use the range walk data in creating a representative received signal $r[n]$, the contents of Fig. 3.13 are read into a MATLAB® workspace using the "imageread" command. Next, data points are backed out by isolating the nearly pure red pixels from the remaining space. In the resulting matrix column location represents range and RCS magnitude (in decibels) is represented in row location. Figure 3.17 is an illustration on a smaller scale of what the matrix might look like. All non-zero values are red pixel (range walk data) locations which may be mapped as shown to the appropriate magnitude. The illustration of Fig. 3.17 finds the mean magnitude (in dB) value for two columns.

In an effort create multiple data sets, this mean along with a standard deviation, both on a linear scale, are calculated for all data columns. Fidelity is limited by pixel size of the original image in this process, so while the measured data used to create Fig. 3.13 contains a sample every nanosecond (roughly $120,000$ samples), this "pseudo-measured" data has only 875 samples, or approximately 1 data point for every 137 nanoseconds. As a result, the mean vector, h_{ave}, and the standard deviation vector σ, both contain 875 data points. Using these vectors, an infinite number of

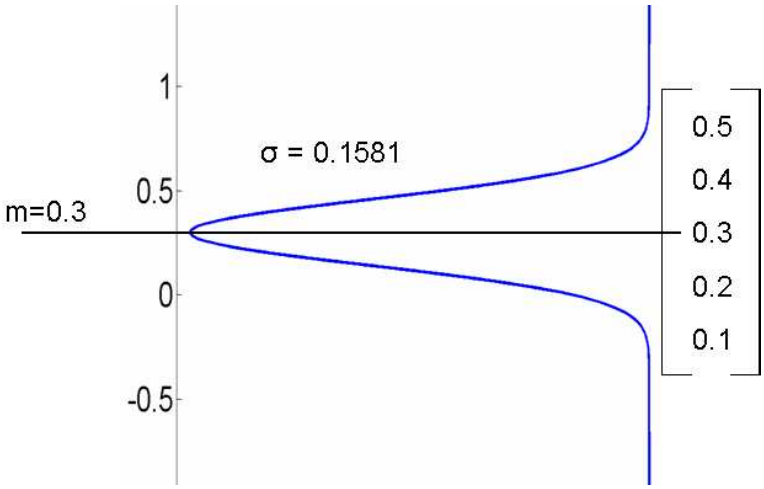

Figure 3.18: Gaussian Magnitude Distribution for Representative Column of the Data Image Matrix

data sets may be formed by employing a Gaussian magnitude distribution for each vector pair ($h_{\text{ave}}[1]$ and $\sigma[1]$, for example). Figure 3.18 shows this process for one data image column. The column vector of linear magnitudes shown are the mapped locations of red pixels from the data image column under consideration. The mean and standard deviation are computed for this range of values, and used to create the distribution shown in blue. This process is repeated to create magnitude values for all 875 samples. For completeness and to introduce complex values which are representative of actual radar signals, a uniform phase distribution, ϕ, is applied as well. The entire process is captured by:

$$h'[n] = H[n]e^{j\phi[n]}, \tag{3.3}$$

where $H[n] \sim N(h_{ave}[n], \sigma[n])$ and $\phi \sim U(0, 2\pi]$.

Figure 3.19 shows 1000 such realizations of $h'[n]$ along with the original data image. This figure was created not by an average of all realizations, but each plotted one at a time without erasing the previous tracings. The intent is to show the range of simulated data falling mostly within the bounds of the image used to create it, which it does.

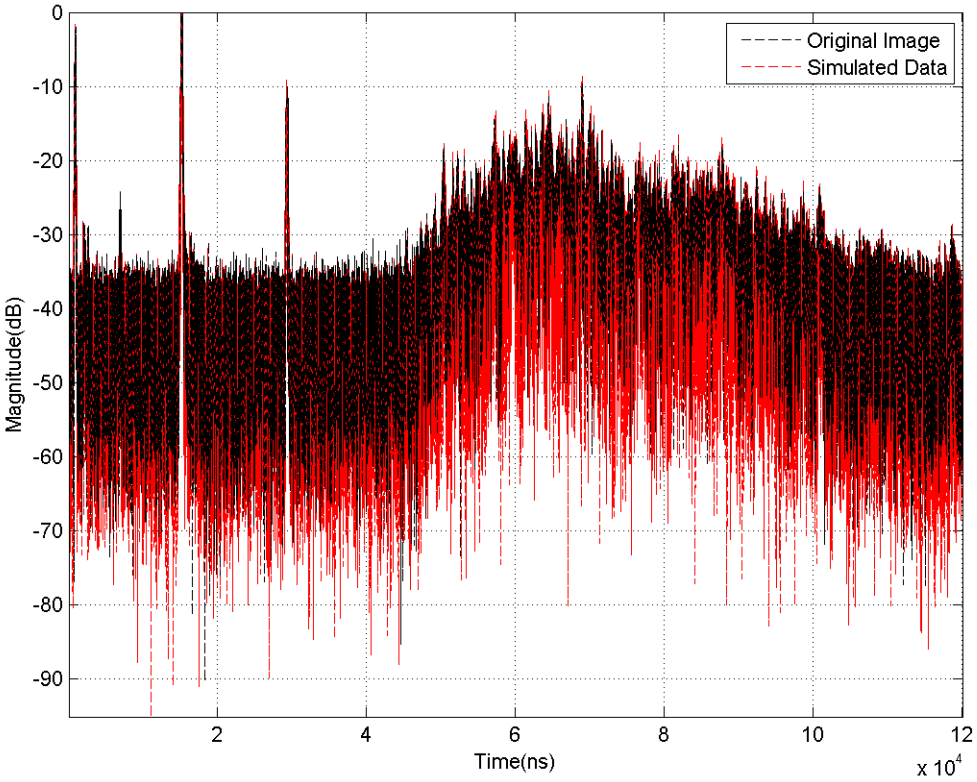

Figure 3.19: Original data image with 1000 realizations of simulated terrain data overlaid.

Now, recall a single data value exists for every 137 nanoseconds in range. It should be noted that a representation more true to the actual environment would have data at every nanosecond increment. Rather than introduce added uncertainty by estimating the remaining data, zero padding was implemented. To maintain appropriate spacing in range, each $h'[n]$ is zero-padded with 136 zeros after each known value. This new vector, $h[n]$ is called the terrain impulse response (TIR).

The received radar signal is created by simply convolving a transmit signal, $s[n]$ with the TIR:

$$r[n] = s[n] * h[n]. \tag{3.4}$$

Since magnitudes of $h[n]$ were extracted from a range vs. magnitude realization, no further accounting of range or power scaling is considered.

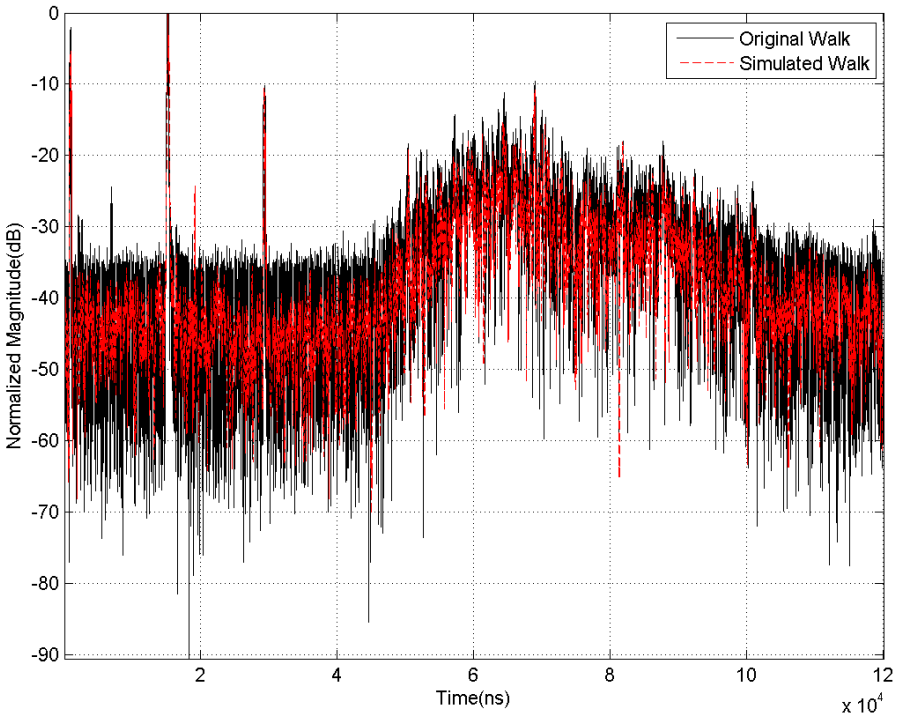

Figure 3.20: Original range walk vs. simulated walk produced by random realization of $h(n)$ and full radar processing.

As a simple test to further validate $h[n]$, an attempt is made to recreate the original range profile in Fig. 3.13. A random realization of the TIR is used, along with an un-coded rectangular pulse, with baseband carrier for $s[n]$, to create a representative $r[n]$. The hope is that match-filtering this received signal will produce a second range profile very similar to the data given. Results of this test are shown in Fig. 3.20. A subtle, yet important difference from Fig. 3.19 is that in this image, *radar processed* data is compared to the original image versus the TIR. Visual examination confirms the desired Gaussian amplitude distribution, as most of the data lies along the mean, with an occasional data point falling outside the bounds of the original data's range.

The terrain is now well characterized and has been used to successfully recreate a range profile using full radar processing. With no target in place at measurement time, the next logical step is to artificially add one to the terrain data.

3.4 Adding a Target Profile

A single point-scatterer would be an easy target representation, but terribly unrealistic for most azimuth angles of most measurement targets. Taking several point scatterers at reasonable separations provides a better representation, but one that is still easily implemented. For example, if an aircraft is measured nose-on with a horizontal polarization, four primary scattering regions would likely contribute to the overall RCS, as illustrated by the stars in Fig. 3.21: radar bulkhead, cockpit, leading wing edges and a combination of aft control surfaces and engine cavity. The overlaid range profile shown in the figure comes from actual measured data of a fighter-size aircraft, and has been blended with NRTF measured data at the appropriate range, as shown in Fig. 3.22. It is assumed that received target signals will have a high enough signal-to-noise ratio (SNR) that the target profile as shown can stand alone. In other words, the portion of the TIR where the target is inserted contains only target data without any added noise. Finally, no phase variation is added over the target portion of the TIR.

With a viable TIR in hand which includes an accurate target representation, the next step is to create multiple data sets for varying target and clutter signal power ratios. This data is eventually used to test the effectiveness of NLS on outdoor RCS measurements.

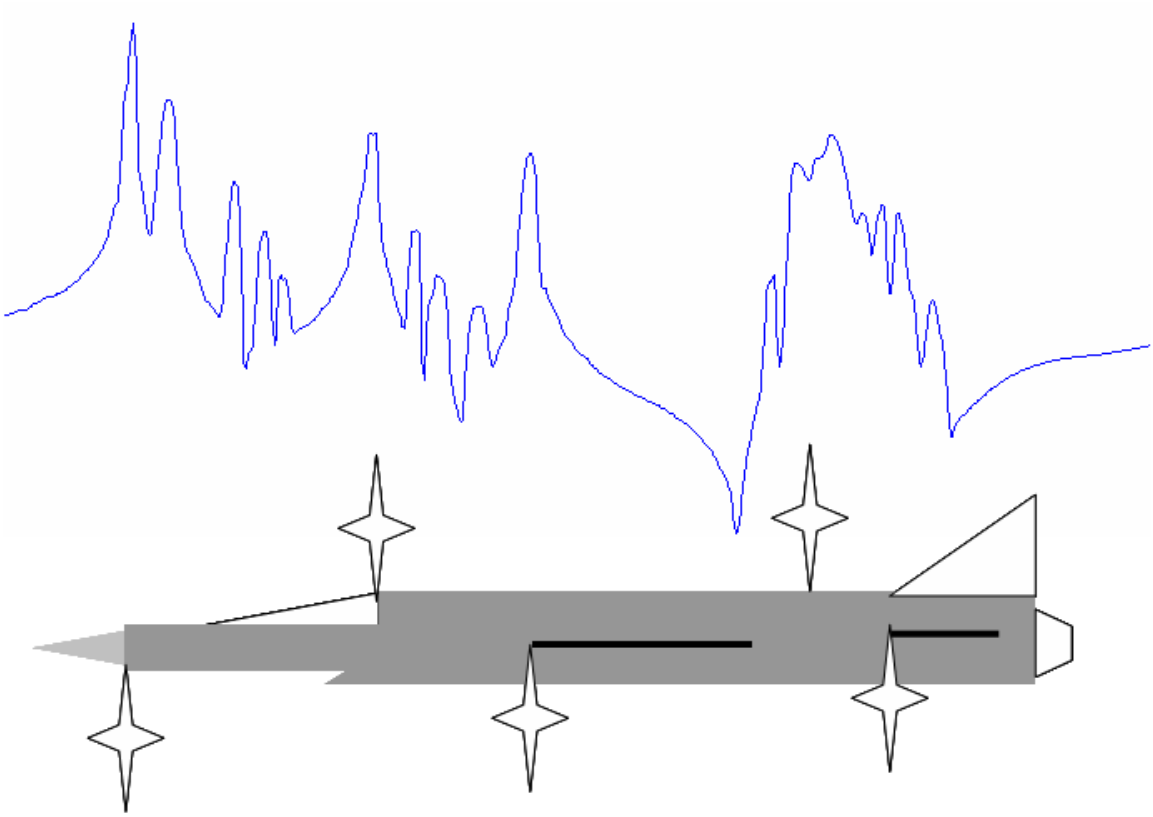

Figure 3.21: RCS Range Profile and Corresponding Scattering Locations for Measurement Target

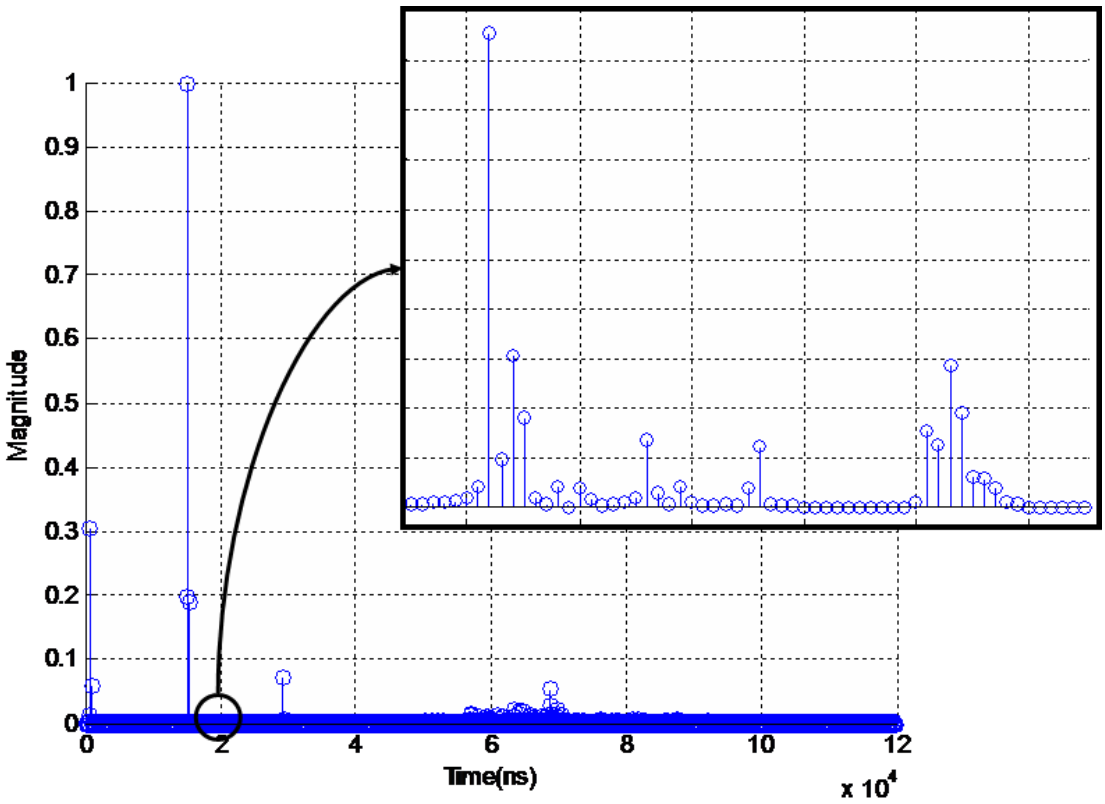

Figure 3.22: Terrain impulse response with target inserted.

IV. Applying NLS to Simulated NRTF Range Data

This chapter details the steps taken to create "pseudo measured" data sets which are used in final simulations. Thresholding techniques are further refined based on multiple measurements, and are used in final performance analysis.

4.1 Creating Final Data Sets

Five cases are again considered for nonlinear suppression (NLS) testing on the simulated National Radar Test Facility (NRTF) range data. To this end, 1000 realizations of the terrain impulse response (TIR) are created for all 5 Input $\frac{P_u}{P_a}$ ratios studied in Chapter III. The aim, for example, in the -6 dB case is to create 1000 realizations with an *average* Input $\frac{P_u}{P_a} = -6$ dB. Recall the relative target amplitudes are fixed (ie. no Gaussian variation), so all that is needed is an average P_a calculated over a representative M = 1000 samples.

$$P_a \text{ ave} = \frac{\sum_{m=0}^{M-1} P_a[m]}{M}. \tag{4.1}$$

With this value in hand, $r_U[n]$, the received unambiguous signal (and therefore P_u), can be adjusted to attain the desired $\frac{P_u}{P_a \text{ave}}$ ratio simply by scaling the magnitude of the target portion of the terrain impulse response, $h_T[n]$, by a constant D.

$$r_U[n] = (Dh_T[n]) * s_U[n] \tag{4.2}$$

Since $r_U[n]$ contains only the target response, it is considered the hardware-gated received unambiguous pulse. The same time duration is used to simulate gating of the ambiguous signal, $r_A[n]$ as well, and the sum of these represents the composite received signal $r[n]$.

$$r[n] = r_U[n] + r_A[n] \tag{4.3}$$

4.2 Setting Thresholds for Final Simulations

Since it is impractical due to sheer volume of simulations to optimize unique threshold scaling constants and sampling widths for each of the 5000 $h[n]$'s, an averaging technique is employed. For the ideal threshold, the scale factor a is adjusted to optimize the total power ratio (TPR) and suppressed power ratio-unambiguous (SPRU) for a received signal generated from the mean TIR, $h_{\text{ave}}[n]$. This value of a is then used to find a unique ideal threshold, termed the floating threshold $\bar{\alpha}$, for all 1000 realizations of each input ratio, which in-turn are averaged to find $\bar{\alpha}_{Fixed}$, the fixed ideal threshold for each ratio. This threshold is then used to perform NLS on all 1000 realizations in each ratio set.

A second method is tested, which simply performs NLS using the floating threshold $\bar{\alpha}$ on each realization. Table 4.1 compares results of both methods. In nearly every case, increase in $\frac{P_u}{P_a}$ at the output was greater for the floating method. Without exception, the floating threshold improved the SPRU, as values were nearer to one in all instances. The suppressed power ratio-ambiguous (SPRA) metric is unremarkable in this comparison, as no perceivable trend is noted. As is the case with the SPRU, all SPRA values for each input ratio are extremely similar for each method.

Although improvement was marginal, an extension of the concept behind the floating average threshold is used in the applied techniques of single local average (SLAT) and multiple local average thresholding (MLAT) as well. In both in-

Table 4.1: Fixed ideal threshold vs. floating ideal threshold performance on distributed target and clutter sources.

	Fixed Ideal Threshold				Floating Ideal Threshold		
Ave Input $\frac{P_u}{P_a}$(dB)	$\Delta\frac{P_u}{P_a}$(dB)	SPRU	SPRA		$\Delta\frac{P_u}{P_a}$(dB)	SPRU	SPRA
-6.07	+6.06	0.939	0.224	$\Rightarrow$	+6.10	0.943	0.223
-3.15	+6.17	0.948	0.222	$\Rightarrow$	+6.18	0.952	0.223
-0.09	+6.18	0.938	0.220	$\Rightarrow$	+6.23	0.941	0.220
2.88	+6.45	0.973	0.220	$\Rightarrow$	+6.46	0.974	0.220
5.87	+6.50	0.967	0.219	$\Rightarrow$	+6.49	0.968	0.220

Table 4.2: Optimized values of TPR and SPRU used in distributed target and clutter NLS testing.

Ave Input $\frac{P_u}{P_a}$(dB)	TPR	SPRU
-6.08	1.49	0.96
-3.15	1.24	0.96
-0.10	1.10	0.96
2.88	1.05	0.98
5.87	1.03	0.98

stances, the scale factor and sampling width are adjusted for optimum TPR and SPRU for the same series of $h_m[n]$ -generated received signals. It is conceded that adjusting thresholds relative to the performance metrics is not feasible in reality, but is done here to reveal potential best-case results.

In cases where the average Input $\frac{P_u}{P_a}$ was negative (ie. clutter power stronger than target), it becomes apparent that a TPR of 1 is impractical. As the TPR approaches 1^+, the SPRU simultaneously trends away from 1, indicating too much target energy is being removed. In all cases, an experimental balance is struck over multiple trials to maximize SPRU while bringing the TPR as near to 1 as possible. Table 4.2 contains the final values the thresholds are adjusted to attain. As implemented in the ideal threshold case, the final scale factor and sampling width values from the optimized SLAT and MLAT are used to generate unique local average thresholds for both techniques, using all $h[n]$ s.

4.3 Final NLS Evaluation

Final NLS evaluation is conducted on the aforementioned 1000 -member data sets for each Input $\frac{P_u}{P_a}$. Table 4.3 shows the final results of the SLAT and MLAT methods compared once again to data obtained using floating ideal thresholds.

While not the focus of this research, it is interesting that the ideal threshold seems to perform poorly in these experiments. In fact, it is surpassed in $\Delta\frac{P_u}{P_a}$ by the other methods in 7 of 10 trials and is outperformed in SPRA for 6 of 10. The ideal

Table 4.3: Floating ideal threshold vs. single local average and multiple local average threshold performance on distributed target and clutter sources. All data shown is an average of 1000 realizations.

	Floating Ideal Threshold				Single Local Ave Thresh		
Input $\frac{P_u}{P_a}$(dB)	$\Delta\frac{P_u}{P_a}$(dB)	SPRU	SPRA		$\Delta\frac{P_u}{P_a}$(dB)	SPRU	SPRA
-6.08	+6.10	0.943	0.223	$\Rightarrow$	+6.68	0.941	0.197
-3.15	+6.18	0.952	0.223	$\Rightarrow$	+6.77	0.955	0.206
-0.10	+6.23	0.941	0.220	$\Rightarrow$	+6.78	0.947	0.205
2.88	+6.46	0.974	0.220	$\Rightarrow$	+6.60	0.933	0.223
5.87	+6.49	0.968	0.220	$\Rightarrow$	+6.21	0.965	0.274

	Floating Ideal Threshold				Multi Local Ave Thresh		
Input $\frac{P_u}{P_a}$(dB)	$\Delta\frac{P_u}{P_a}$(dB)	SPRU	SPRA		$\Delta\frac{P_u}{P_a}$(dB)	SPRU	SPRA
-6.08	+6.10	0.943	0.223	$\Rightarrow$	+6.35	0.923	0.205
-3.15	+6.18	0.952	0.223	$\Rightarrow$	+6.41	0.917	0.206
-0.10	+6.23	0.941	0.220	$\Rightarrow$	+6.45	0.914	0.208
2.88	+6.46	0.974	0.220	$\Rightarrow$	+6.43	0.924	0.227
5.87	+6.49	0.968	0.220	$\Rightarrow$	+6.06	0.936	0.271

threshold did perform well in the SPRU metric, being nearer to 1 in all cases compared to the MLAT, and 3 of 5 against the SLAT. This slip in performance relative to the other methods is possibly explained by re-examining Fig. 3.2. A threshold following so closely to the contour of the dispersed target pulse may create problems when applied to distributed clutter sources. Gated signals which contain multiple clutter sources provide increased opportunities for the composite signal to exceed the threshold when match-filtered to the clutter waveform, which subsequently removes excessive data. Figure 4.1 illustrates this concept with multiple potential sources of error enclosed by circles.

When comparing the single- and multiple-thresholding techniques to each other, it is quickly apparent that SLAT performance is superior if the intent is to simply gather RCS magnitude data. The SPRU for the single threshold-processed data is nearer to 1 for all input $\frac{P_u}{P_a}$ ratios and the SPRA is closer to 0 in 3 of 5. Finally, the $\Delta\frac{P_u}{P_a}$ is on average 0.268dB greater in the SLAT trials as well. While somewhat

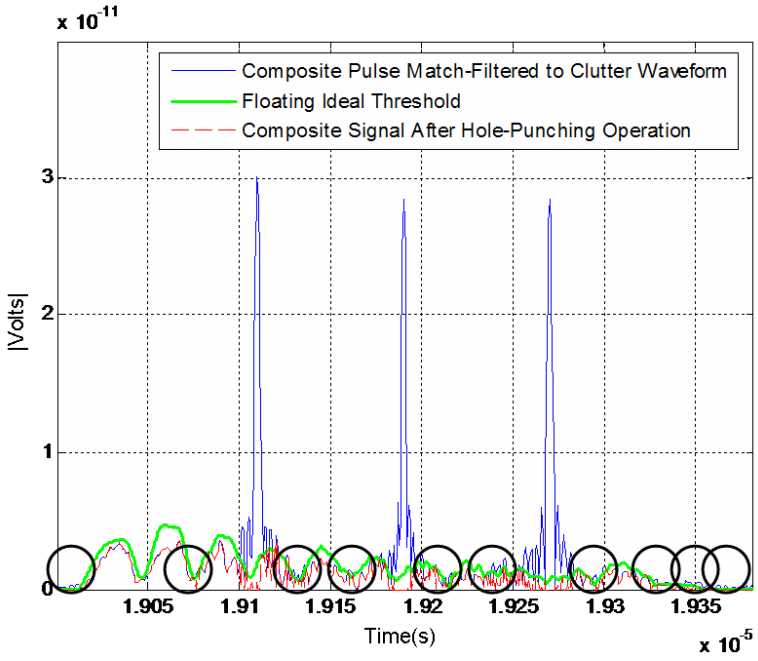

Figure 4.1: NLS using the floating ideal threshold for one realization of h[n], input $\frac{P_u}{P_a} = -6$dB. Circled regions represent areas where potentially too much signal power is removed due to the close mapping of the ideal threshold to the dispersed target pulse.

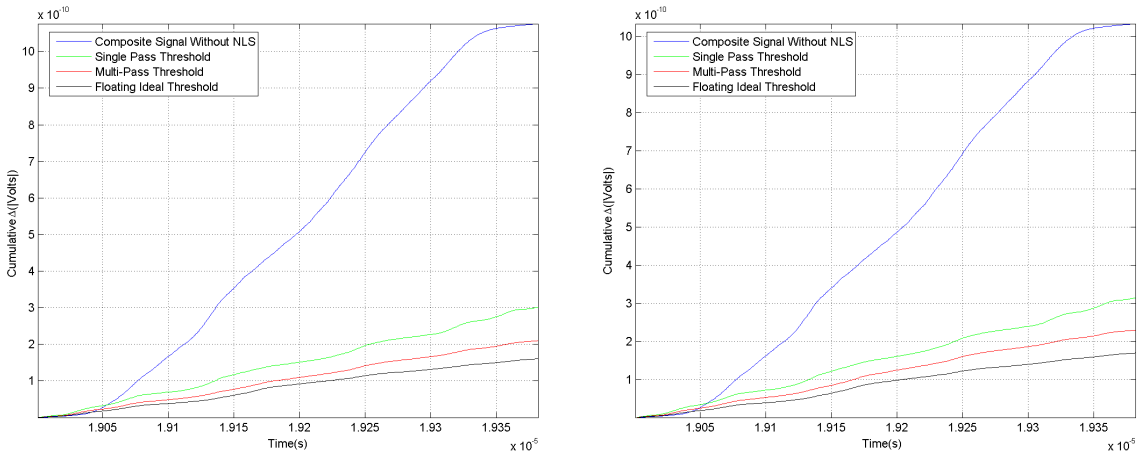

(a) (b)

Figure 4.2: Cumulative point-by-point $|\Delta|$ for all thresholding techniques. The $|\Delta|$ is measured from a match-filtered target pulse, and reveals how well NLS-processed waveforms follow the contour of "pure" data. All thresholds adjusted for optimum TPR and SPRU.
(a) Average Input $\frac{P_u}{P_a} = -6.08$dB
(b) Average Input $\frac{P_u}{P_a} = -3.15$dB

counter-intuitive, Figs. 4.2 through 4.4 reveal that NLS using the MLAT technique, while outperformed in nearly all metrics, may continue to have promise in imaging applications. On the surface it appears on average that too much target energy and not enough clutter energy is removed. The apparent benefit of the MLAT technique is that these energies seem to be largely removed or maintained in the right places, which is evident from the lower cumulative error seen in the figures.

In contrast to the experiments in Chapter III, the change in $\frac{P_u}{P_a}$ now decreases as power of the clutter return increases for the ideal threshold cases. This time the change does indeed appear to be indicative of improved performance, as SPRU values show a decreasing trend and SPRA increases as the clutter becomes stronger.

The applied techniques of single and multiple local average thresholding in unison follow but one trend: as clutter strength decreases, SPRA increases. This tendency makes good sense intuitively, as a weakening clutter response will blend more readily with the dispersed target response, and therefore be more difficult to remove.

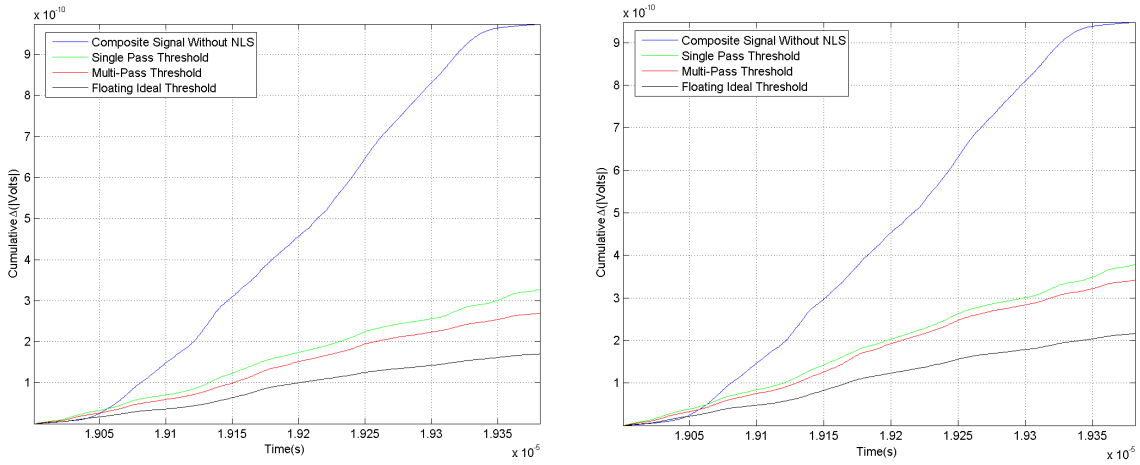

(a) (b)

Figure 4.3: Cumulative point-by-point $|\Delta|$ for all thresholding techniques.
(a) Average Input $\frac{P_u}{P_a} = -0.10$dB
(b) Average Input $\frac{P_u}{P_a} = 2.88$dB

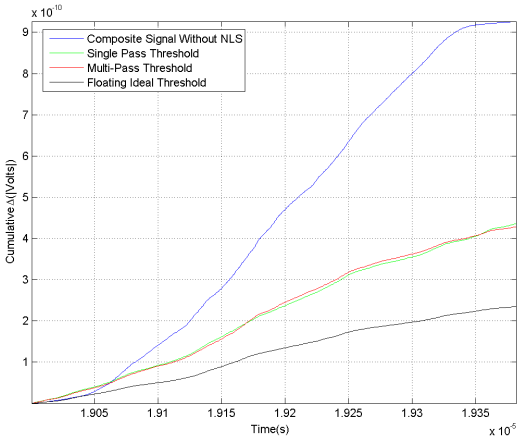

Figure 4.4: Cumulative point-by-point $|\Delta|$ for all thresholding techniques. Average Input $\frac{P_u}{P_a} = 5.87$dB.

The results presented make a strong case for the viability of using nonlinear suppression in RCS measurements. If considering the SPRA and SPRU as simple percentages as proposed in Chapter II, on average the MLAT technique removed 78% of clutter power while maintaining 92% of target power. Better still are the single thresholding technique results. An identical average of 78% clutter power is removed with 95% target power retention.

V. Conclusions

This chapter highlights material presented and the subsequent results. Finally, suggestions for future research are presented which would further demonstrate the benefit of nonlinear suppression (NLS) in the outdoor measurement facility.

5.1 Summary and Contributions

It is important to realize that in an actual measurement scenario, it is completely impractical and even nonsensical to apply the ideal threshold. The ideal threshold is only introduced here as part of performance evaluation. If implemented, the user needs to collect a single unambiguous pulse for every azimuth of the target measured to establish threshold values. This is obviously impractical, as it completely eliminates the need for NLS. The purely unambiguous pulse response is indeed the truth data that the process is attempting to recover.

On the other hand, NLS using multiple or single local average thresholding shows considerable promise. Potentially, if complex data is saved for post-processing, a wide range of input unambiguous to ambiguous power ratios ($\frac{P_u}{P_a}$) can be characterized. Conceivably, optimized threshold scaling and sampling widths for a given $\frac{P_u}{P_a}$ could be developed using calibration targets of known RCS, and subsequently applied to future measurement scenarios. An a priori estimate of the target's radar cross section (RCS) is obviously a must in this proposition. This estimate is potentially accomplished by first taking spot measurements at a low pulse repetition frequency for several key customer-defined threat sectors, in a calibration stage of sorts. Separately integrating 1000 ambiguous, followed by 1000 unambiguous pulses would mimic the data used in this thesis, and could be used to select the appropriate optimized thresholding constants.

NLS is not proposed as the only solution to mitigating long-range clutter at outdoor RCS measurement facilities. However, it does provide a level of promise worthy of further investigation.

5.2 The Way Ahead

Linear frequency modulated (LFM) waveforms, while lending themselves nicely to this research, are likely not the best choice for RCS measurements which tend to be frequency sensitive. Additionally, as eluded to in Chapter I, a continuous LFM pulse is currently not even in the suite of available waveforms at the National Radar Test Facility (NRTF). While a stepped LFM (pulse-to-pulse) is available for increasing frequency, a decreasing step is not. A subsequent round of experiments using phase-coding techniques such as Gold or simulated annealing-generated codes would perhaps provide a more realistic, realizable approach for NRTF. In contrast to LFM, these code families have multiple members which would allow for more than two channels in the NLS model [1]. This flexibility would allow the user to increase the PRF which decreases measurement times and ultimately saves dollars.

Bibliography

1. Anderson, Jon M. *Nonlinear Suppression of Range Ambiguity in Pulse Doppler Radar*. Ph.D. dissertation, Graduate School of Engineering, Air Force Institute of Technology (AETC), Wright-Patterson AFB OH, April 2001. AFIT/DS/ENG/01-05.
2. Hale, Todd B. "Class Notes", June 2005. EENG668, Advanced Radar Systems.
3. Skolnik, Merrill I. *Introduction to Radar Systems*. McGraw-Hill, New York, NY, third edition, 2001.

REPORT DOCUMENTATION PAGE

Form Approved
OMB No. 0704–0188

1. REPORT DATE *(DD–MM–YYYY)*	2. REPORT TYPE	3. DATES COVERED *(From — To)*
23–03–2006	Master's Thesis	Sept 2004 — Mar 2006

4. TITLE AND SUBTITLE

Nonlinear Suppression
of Range-Ambiguous Clutter
for Outdoor Radar
Measurement Facilities

5a. CONTRACT NUMBER

5b. GRANT NUMBER

5c. PROGRAM ELEMENT NUMBER

6. AUTHOR(S)

Michael C. Baumgartner, Capt, USAF

5d. PROJECT NUMBER

5e. TASK NUMBER

5f. WORK UNIT NUMBER

7. PERFORMING ORGANIZATION NAME(S) AND ADDRESS(ES)

Air Force Institute of Technology
Graduate School of Engineering and Management (AFIT/EN)
2950 Hobson Way, Bldg 640
WPAFB OH 45433-7765

8. PERFORMING ORGANIZATION REPORT NUMBER

AFIT/GE/ENG/06-06

9. SPONSORING / MONITORING AGENCY NAME(S) AND ADDRESS(ES)

46th Test Group/NRTF, Air Force Materiel Command
871 Dezonia Dr
Holloman AFB, NM 88330
POC: Mr. James H. Eggleston, Technical Director
James.Eggleston@46tg.af.mil, DSN: 349-3323

10. SPONSOR/MONITOR'S ACRONYM(S)

11. SPONSOR/MONITOR'S REPORT NUMBER(S)

12. DISTRIBUTION / AVAILABILITY STATEMENT

Approval for public release; distribution is unlimited.

13. SUPPLEMENTARY NOTES

14. ABSTRACT

In the outdoor measurement facility, a certain amount of real estate is owned by the organization, and therefore can be groomed to keep clutter contributions to a minimum. As the transmit signal travels further downrange, however, returns from long-range clutter sources are inevitable, and can have significant impact on measurement accuracy. This research effort investigates the effectiveness of employing nonlinear suppression (NLS) to abate long-range ambiguous clutter in these facilities. Initial testing provides an extended proof-of-concept for coincident point scatterers representing target and clutter sources. The NLS process is finally applied to simulated measured data from the National Radar Test Facility (NRTF), where five cases representing various target versus clutter signal power ratios are tested. Ratios are selected to cover the range of clutter signals having 0.25 times the power to 4 times the power of the target signal. Results show promise for employing NLS in this arena, as one of the techniques studied retained on average 95 percent of the target signal power while discarding 78 percent of the ambiguous signal power.

15. SUBJECT TERMS

radar, nonlinear suppression, range ambiguity, clutter suppression, radar cross section measurement

16. SECURITY CLASSIFICATION OF:			17. LIMITATION OF ABSTRACT	18. NUMBER OF PAGES	19a. NAME OF RESPONSIBLE PERSON
a. REPORT	b. ABSTRACT	c. THIS PAGE			Todd B. Hale, Maj, USAF
U	U	U	UU	59	19b. TELEPHONE NUMBER *(include area code)* (937) 255–3636, ext 4639